International Journal of Material Forming (2025) 18:16
https://doi.org/10.1007/s12289-025-01879-7

ORIGINAL RESEARCH

Local High Pressure Torsion: a process for creating targeted heterogeneities in metallic materials

E. Beygelzimer[1] · O. Davydenko[2,3] · Y. Beygelzimer[2] · Y. Tereshchenko[1] · V. Bondarchuk[3] · V. Shyvaniuk[3] · R. Fataiev[1] · I. Shapiro[1] · V. Balakin[4] · N. Biba[5] · D. Orlov[6]

Received: 13 October 2024 / Accepted: 27 January 2025 / Published online: 10 February 2025

Abstract
In the light of recent developments in the design of structural materials, micro-architected heterogenous-structure metals are considered among most structurally efficient. In this work, a new technique for Local High Pressure Torsion (L-HPT) enabling the creation of heterogeneous structures through localised deformation processing in sheet metals by impeding a rotating punch is proposed. Using AA5083 aluminium alloy as an example, we show experimentally that the rotation of the punch sets adjacent material layers in motion. This results in more than two-fold increase in material hardness over initial level in the workpiece bulk with rather sharp gradients in hardness level transition. The maximum hardness is observed at the peripheral edge of a punch tip. Finite-element modelling of the L-HPT process confirmed that the rotational flow of workpiece material leads to the accumulation of shear strain. The level of accumulated strain increases with an increase in friction at the contact surface. Further analysis based on dimensionality theory revealed that for such an L-HPT configuration the level of equivalent strain is directly proportional to the ratio of rotation-to-translation speeds at the punch.

Keywords Local High Pressure Torsion (L-HPT) · Deformation processing · Architected microstructures · Gradient structure · Finite element modelling · Friction factor

Introduction

Modern technology demands the creation of metallic materials with unique properties that can be tailored at both micro and macro levels [1]. One of the most efficient approaches to achieving this is the formation of heterogeneities in the surface layers of metallic workpieces through local plastic deformation [2]. It is important to note that the creation of such macroscopic heterogeneities encompasses the formation of microscopic heterogeneities since these scale levels are interconnected concomitantly contributing to the improvement of the mechanical properties in materials [3–5].

Recently, various approaches for the targeted creation of surface heterogeneities, such as Shot Peening, Surface Mechanical Attrition Treatment, Burnishing, Deep Rolling, etc. have been developed [6, 7]. Such methods belong to the processes of 'cold' local plastic deformation, while 'hot' local plastic deformation is implemented through the process of Friction Stir Processing (FSP) [8, 9]. Each of these methods has advantages and disadvantages, while all these methods may lead to the formation of surface defects such

✉ D. Orlov
dmytro.orlov@lth.lu.se

1 OMD-Engineering LLC, 5b Yevropeiska Str, Dnipro 49000, Ukraine

2 Donetsk Institute for Physics and Engineering named after O.O. Galkin, National Academy of Sciences of Ukraine, 46 Nauky Ave, Kyiv 03028, Ukraine

3 G.V. Kurdyumov Institute for Metal Physics, National Academy of Sciences of Ukraine, 36 Academician Vernadsky blvd, Kyiv 03142, Ukraine

4 Ukrainian State University of Science and Technology, 2 Lazaryana Str, Dnipro 49010, Ukraine

5 MICAS Simulations Ltd, Temple Court 107 Oxford Road, Oxford OX4 2ER, UK

6 Division of Mechanics, Materials and Component Design, Department of Industrial and Mechanical Sciences, Faculty of Engineering (LTH), Lund University, Ole Römers väg 1, Lund 223 63, Sweden

as microcracks. On one hand, the cold processes improve the strength and fatigue resistance of materials, as well as increase their wear resistance [6, 10]. On the other hand, the hot process of FSP enables for deeper changes in the microstructure without significant surface defects, while improving the strength and ductility of a workpiece. Besides that, FSP may lead to undesirable phase transformations and the formation of oxides and other undesirable products in some types of materials [11].

Recent interest to surface processing is further elevated by the possibilities for creating gradient-structures opening new opportunities for overcoming the strength-ductility trade-off [12]. In both the cases, significant improvement in workpiece performance is achieved through the localised low-temperature plastic deformation within surface vicinity. The resulting performance improvements can be attributed to the synergy of several factors often studied in isolation. These include such well-known factors as the formation of compressive residual stresses and significant reduction of stress concentrators on the surface [13], and more recently discovered extreme grain refinement and hetero-deformation induced strengthening [14]. In fact, latest discoveries within the latter demand further in-depth investigations of strengthening mechanisms along with the development of new surface processing methods. These can enable additional opportunities for controlling localised plastic deformation and multiscale phenomena in gradient structures.

All the aforementioned processes fall into the category of Severe Plastic Deformation (SPD) characteristic of imposing simple-shear deformation mode under high pressure [15]. The effects of the latter are well understood by now and are known for leading to the intense refinement of grain structure [16, 17], stochastic rotational movements ("solid-phase turbulence") [18], and most importantly significant enhancement of materials properties and even the creation of new materials [19].

These capabilities expand with the increase of maximum achievable simple-shear deformation. Therefore, the development of new processes for local plastic deformation that enable for increased simple-shear deformation in the workpiece surface is of great interest. This is particularly relevant for cold deformation processes maximising the potential for mechanical properties improvement.

In this paper, we propose a new technique for the cold localised plastic deformation processing of surface in metallic materials, which is based on the impingement of a rotating punch. Unlike deep rolling, rotational motion (stirring) of surface layers in the material is induced by the rotational motion of the punch. The rest of workpiece material volume remains virtually intact, which leads to shear straining. The latter can be controlled through the punch rotation parameters to obtain desired performance characteristics. By the principle of cold plastic deformation with simple shear induced by the punch rotation, this process resembles High Pressure Torsion (HPT) [20]. Since deformation in the proposed technique is localised (unlike that in HPT), we call it Local High Pressure Torsion (L-HPT).

L-HPT schematically resembles also FSP [9] while differentiates itself by temperature in the deformation zone, which can be classified as 'cold' and associated specific phenomena. The absence of significant material warming in L-HPT is controlled by relatively low speed of punch rotation, which is 2–3 orders of magnitude less than that in FSP while on parity to rotational speeds in HPT.

A critical condition for realising L-HPT is the gripping of surface layers in the metal substrate with the punch, which is far from guaranteed by default. With a reference to HPT, full capture of a workpiece surface by a punch is only possible when the stress on contact friction reaches the level of plastic shear stress in the material [21]. This condition is not always fulfilled in HPT, which leads to the workpiece slippage and associated arrest of plastic deformation [22, 23].

The main goals of this paper are to introduce the concept of L-HPT, to demonstrate the conditions for the workpiece material gripping by a rotating punch, and to assess the maximum equivalent strain, which can be achieved through a single pass in this process. The detailed investigation of process variables and their effect on stress-strain state in the workpiece as well as the analysis of microstructures and material performance characteristics obtainable by L-HPT are reserved for the follow-up publications.

Concept of L-HPT

The schematic of L-HPT is presented in Fig. 1, which shows a punch 1 inserted into a plate 2 under a pressure P and is rotated with a torque M. Note the processing tool for L-HPT is reasonable to call a punch, not a die as in HPT, since it impinges into the plate.

The L-HPT process can be implemented both with and without the moving of the punch within the $X-Y$ plane (RD-TD in Fig. 1).

Experimental materials and methods

Experimental material

The material in this study was an aluminium alloy AA5083 having the nominal chemical composition as following (in wt%): Mg 4,81%; Mn 0,53%; Fe 0,32%; Cu 0,07%; Si 0,09%; Cr 0,10%; Zn 0,02%; Ti 0,01%; Al balance. The plates (workpieces) for processing had the dimensions of

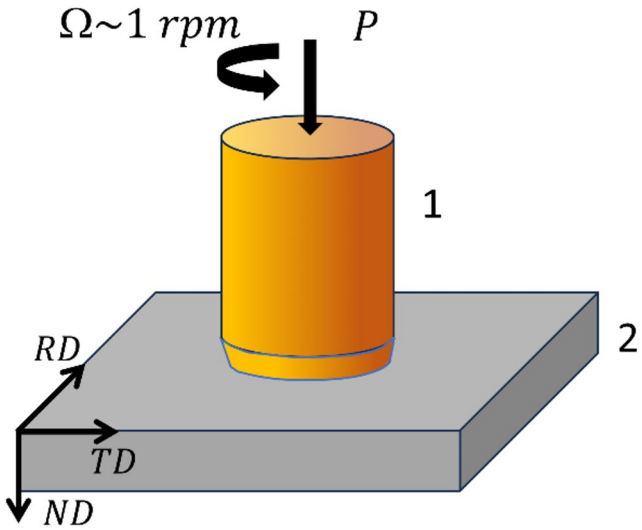

Fig. 1 Schematic drawing of L-HPT: 1- punch, 2- plate, Ω- angular velocity, *P*- compressive pressure on the punch, RD, TD and ND are rolling, transverse and normal directions, respectively in the reference system of as-supplied plate (after rolling)

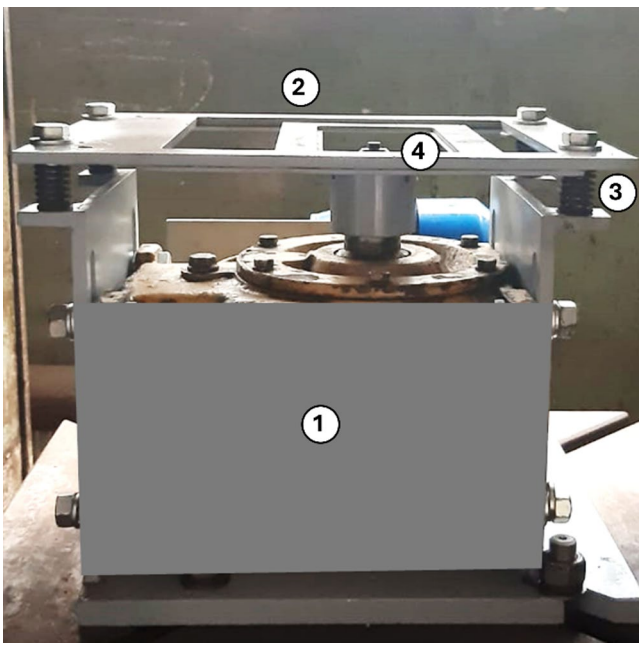

Fig. 2 Photograph of the L-HPT toolset unit: (**1**) electric motor with a gearbox for the punch rotation, (**2**) frame for holding and positioning the workpiece, (**3**) spring-loaded guides, (**4**) rotating punch

$9 \times 70 \times 70 mm^3$ and were cut from a hot rolled strip heat treated following ASTM H116 regime. The initial microhardness of the workpieces was HV 100.

L-HPT processing method

The processing of the workpieces was carried out at the L-HPT toolset developed at OMD Engineering (Dnipro, Ukraine), see Fig. 2. The toolset is designed in the form of a unit installed on the lower plate of a hydraulic press having a maximal compressive force of 1 MN. The unit contains an electric motor with a gearbox for the punch rotation. The maximum torque on the gearbox output shaft is 700 Nm, and the angular rotation velocity can be varied between 1 and 5 rpm with a step of 1 rpm. The forward speed of the press plate is controlled by a choke in the range from 0.1 mm/s to 2.0 mm/s.

A frame for the holding and positioning of the workpiece is mounted on top of the punch on four spring-loaded guides. When the upper plate of the press is lowered, the frame moves down, and the rotating punch is impinged into the workpiece. The toolset allows controlling penetration depth into the workpiece along with compression force and torque on the punch. The punch had a stair-shape edge, as shown in Fig. 3 to limit the depth of penetration into the workpiece. Studying he effects of the punch and the tip shapes are reserved for the follow-up studies.

Immediately before L-HPT processing, workpiece surface was degreased with 96%-pure ethanol. After that, the workpiece was mounted on the frame and lowered with the press plate at a speed of 0.1 mm/s until contact with a compression force at a punch of 0.3 MN. The punch rotating at an angular velocity of 5 rpm was impinged in the workpiece for the full depth of the tip stair. The total angle of punch rotation was 3.3 revolutions.

Metallographic specimen preparation and characterisation

Immediately after the L-HPT processing specimens for microstructure characterisation and microhardness measurements were cut from the workpiece in both RD-TD and ND-TD sections. Afterwards, the specimen surfaces were mechanically ground on SiC paper down to grit 2000 and polished with diamond suspension to particle size of 1 μm.

The microstructure was examined by scanning electron microscopy (SEM) using a Tescan VEGA3 SEM with tungsten filament. The accelerating voltage was 20 kV, beam current between 100 pA −2 nA, and a nominal working distance between 7 and 15 mm. Unless otherwise specified, all the micrographs below represent back-scattered electron (BSE) images in compositional (atomic-number) contrast. Local chemical composition was determined by energy dispersive spectroscopy (EDS) using Bruker XFlash Detector 610 M mounted at the same microscope.

Vickers microhardness (HV) measurements were carried out on the same specimens using PMT-3 instrument with a load of 50 g for 10 s. The centre-to-centre distance between the indents in HV mapping was at least three times the diagonal length of measured imprints, and the distance from the

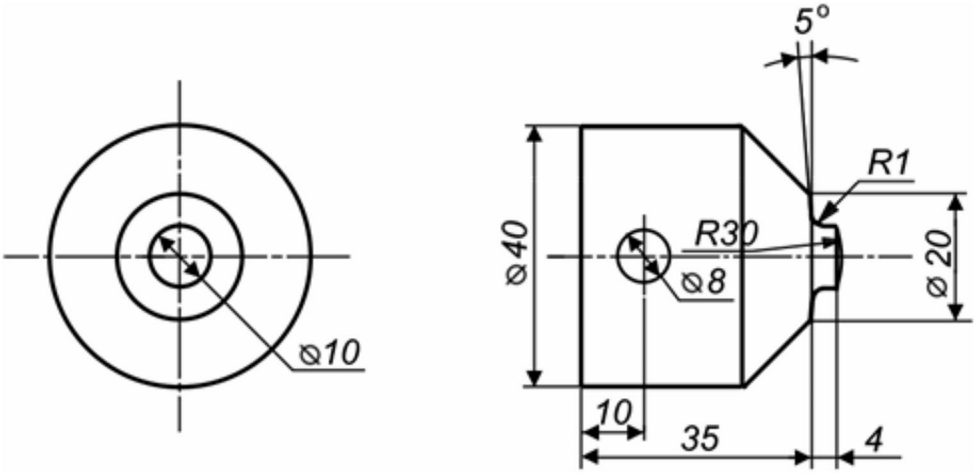

Fig. 3 The sketch of a punch in L-HPT

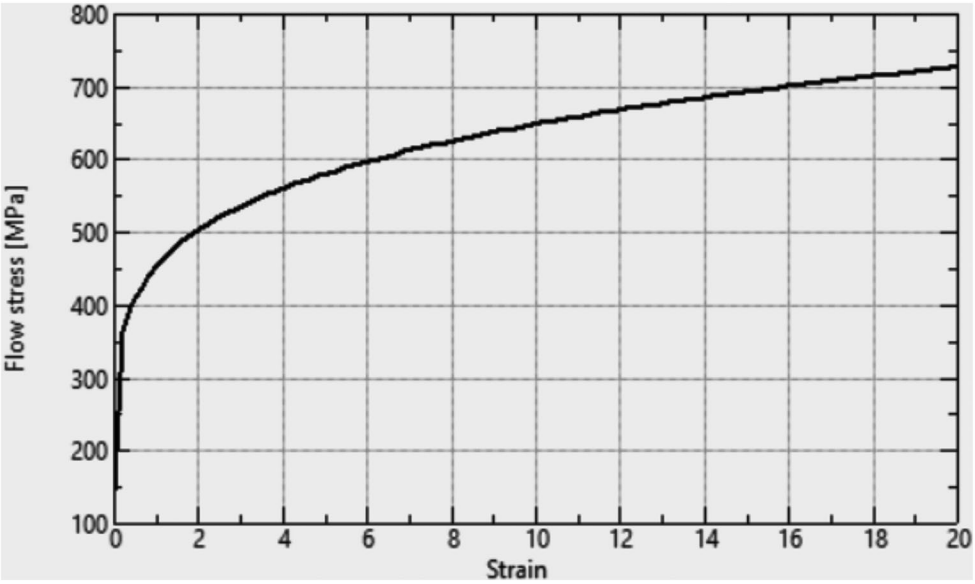

Fig. 4 Stress-strain curve for the alloy AA5083 H116 following Eq. (1), which was used for the FE simulations in QForm

centre of an indentation to the edge of the specimen was at least 2.5 times the diagonal length.

Method of finite-element (FE) simulations

Numerical simulations were carried out using a commercial software suite QForm-3D (v. QForm UK 10.3.1) [24]. Three-dimensions (3D) geometrical model of L-HPT was made identical to the schematic in Fig. 1. The workpiece plate was initially automatically segmented into a mesh consisting of 13 227 four-node tetrahedral finite elements. The mesh was automatically reconfigured during the simulation when the elements were becoming strongly distorted at large strains. As a result, final mesh contained up to 67 885 elements. The material was considered elastic-plastic, and von Mises yield criterion was implemented. Material rheology was modelled using experimental stress-strain curves of the alloy AA5083 H116 from ref [25]. :

$$\sigma_s = \sigma_0 \left(1 + \left(\frac{e_p}{Q_0}\right)^{1/N}\right) \tag{1}$$

where $\sigma_0 = 123.0MPa$, $Q_0 = 0.007$, and $N = 5.06$ are the material parameters for initial yield stress, hardening coefficient and hardening exponent, respectively. e_p is the effective plastic strain. Respective stress-strain curve for the alloy AA5083 H116 is shown in Fig. 4.

Contact friction stress τ_{fr} between the punch and the workpiece was given in the form:

$$\tau_{fr} = mk, \tag{2}$$

where $m \leq 1$ is the friction factor [26]. According to [27],

$$m = f\left(1 - exp\left(1.25q/\sigma_s\right)\right), \tag{3}$$

where q is a normal pressure.

The values of function m in such simulations must but discussed in more detail. In the finite element analysis of HPT, it is necessary to increase the factor m up to 1.5 [28] in order to ensure the adhesion of the sample to the die. With the values of the friction factor $m \leq 1$, the calculations show the slippage of a workpiece relative to the dies, which results in a limitation of the maximum achievable strain [28, 29]. The assumption of $m > 1$ is an artificial technique, which can be justified in solving the problems of plastic deformation with variational methods, in particular with FE, that cannot guarantee that the calculated value of shear stress on the tool surface is equal to the value of friction stress. Indeed, in the power functional to be minimized, τ_{fr} simply determines its proportion due to friction, but is not a boundary condition to be satisfied exactly, as in solving problems with the method of slip lines [30]. Therefore, the values of $m > 1$ in the FE simulations of HPT should be considered as an increase in the penalty of slipping for the material on the die surface.

We used this technique and considered two options: $m = 1$ and $m = 1.5$.

The vertical feed of the punch was carried out at a constant velocity of 0.1 mm/s, and the rotation was carried out at a velocity of 5 rpm up to 3.3 revolutions.

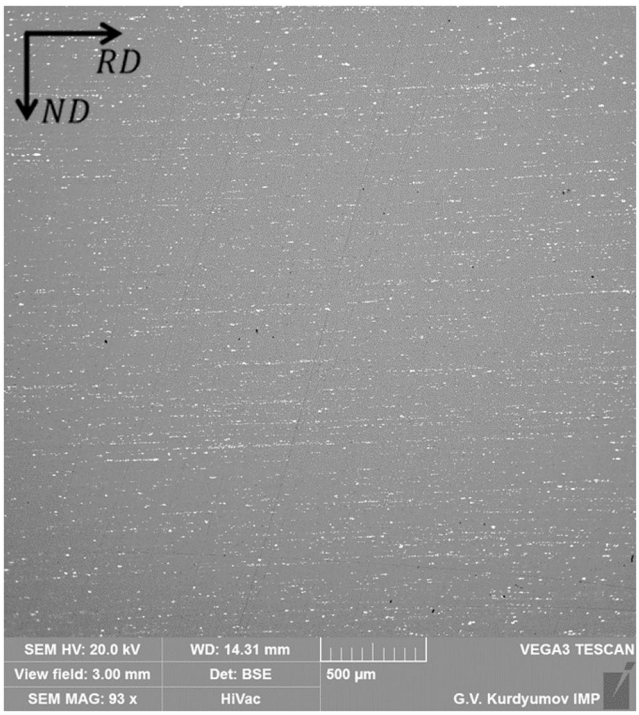

Fig. 5 SEM-BSE micrographs of particle structure in AA5083 H116 alloy in as-supplied condition before L-HPT processing

Experimental and simulation results

Characterisation of microstructure

The representative microstructure of the workpiece before L-HPT processing is shown on RD-ND plane in Fig. 5. The BSE-SEM micrograph in Fig. 5 reveals the strides of bright-contrast particles elongated in rolling direction (RD). EDS analysis indicates their composition consisting of Al–Fe–Mn, which is consistent with the nominal alloy composition and earlier reports on the same material in the literature, e.g., [31]. Such strides of particles can be used as tracers reflecting the flow pattern of a material in plastic deformation processing in general and L-HPT in particular.

Figure 6 shows the evolved particle structures of the alloy in two mutually perpendicular sections of the workpiece plate after L-HPT processing. The strides of particles on the RD-ND section reveal a smooth flow of the material over the punch in vertical direction, area 1 in Fig. 6. In-plane section (RD-TD) reveals a circular movement of the material along the punch periphery, areas 2 and 3 in Fig. 6. In the latter areas, a transition from the circular flow around the punch to unaffected by L-TH particle strides aligned in RD can also be traced. For convenience, this transition is highlighted by yellow dash-lines in the areas 2 and 3, Fig. 6, solid yellow line arc indicates the edge of the punch.

These results confirm that the workpiece plate material can be engaged and dragged by the rotating punch, which causes additional plastic flow when compared to the case of punch impingement without rotation. To investigate the effect of such plastic deformation further, we carried out the mapping of microhardness evolution around the punch after L-HPT.

Microhardness mapping

The distribution of microhardness in representative critical directions in the vicinity of the punch after L-HPT processing is shown in Fig. 7. First, it indicates significant monotonic gradients in HV distribution from the base-line level of HV 100 corresponding to as-supplied material in the areas beyond 4 mm away from the punch to elevated hardness up to HV 235 in the immediate vicinity of the punch. Second, significant gradients in HV distribution along immediate punch periphery can also be found with a minimum value of HV 118 around the punch axis, sharply increasing to a maximum value of HV 235 at the peripheral edge of a punch tip, and gradually decreasing along the tip height to HV 129 at the plate surface.

Such gradients in HV distribution evidence (i) large strain hardening in the material due to L-HPT processing, and (ii) significant dependence of strain hardening on punch

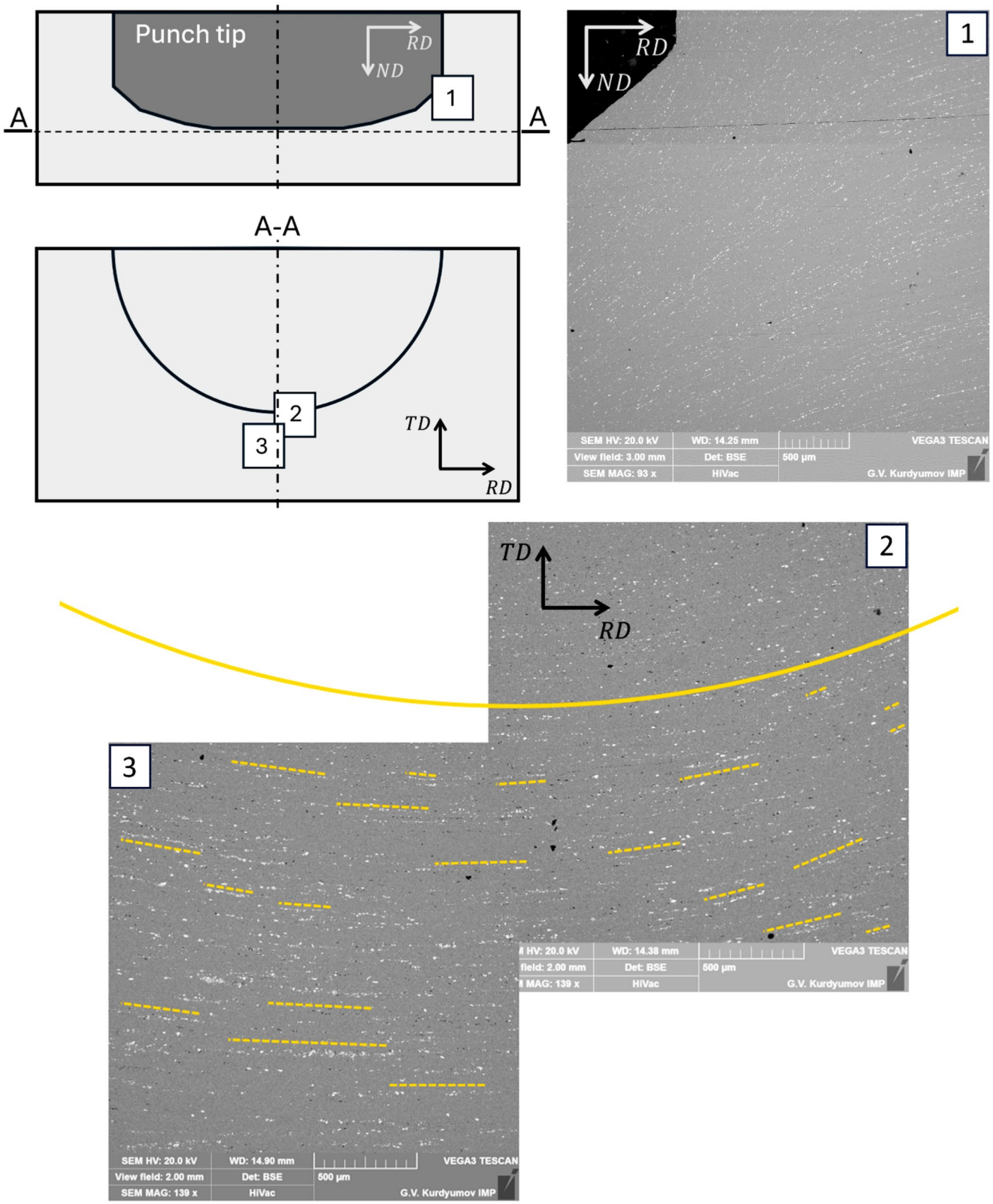

Fig. 6 SEM-BSE micrographs of particle structure in AA5083 H116 alloy evolved after L-HPT processing. Schematics in the top-left corner indicate sections for microstructure analysis with respect to L-HPT processing reference frame and the specific area of observations marked with numbers 1–3. In the areas 2 and 3, solid yellow line arc indicates the edge of the punch, while yellow dash-lines facilitate observation of the direction of metal plastic flow

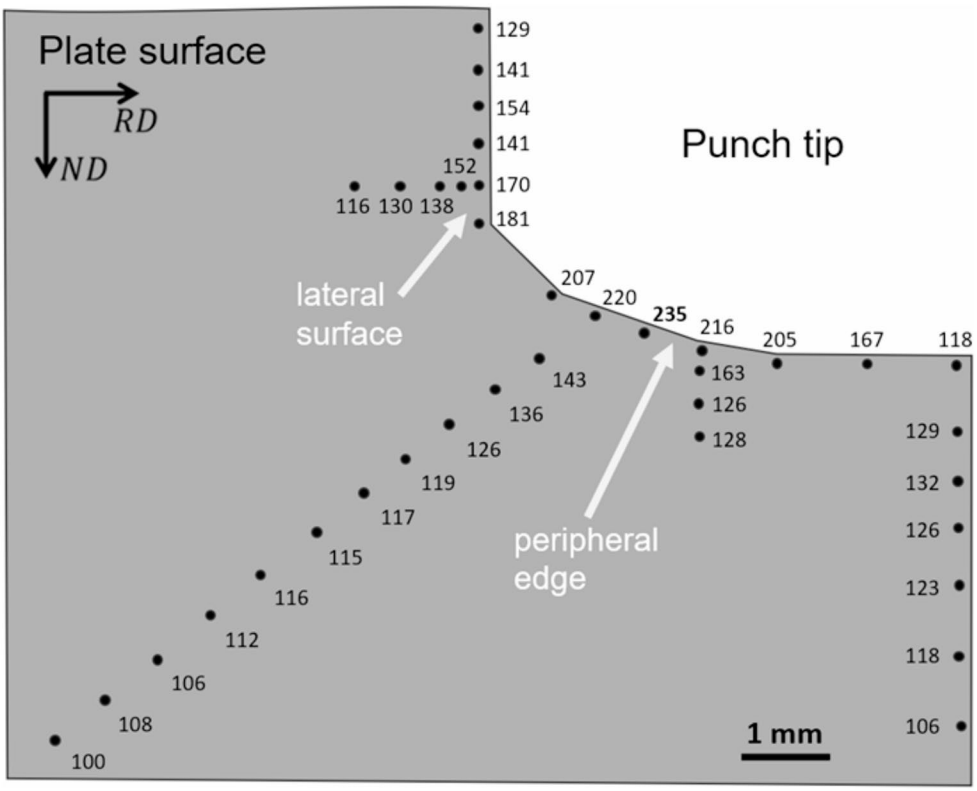

Fig. 7 Distribution of microhardness in the vicinity of the punch after L-HPT processing

geometry as well as rotation angle. In order to understand the evolution of microstructure and corresponding strain hardening in-depth, numerical simulations of plastic flow and strain accumulation during L-HPT were carried out, as presented in the next subsection.

Numerical simulations

The results of numerical simulations with FE method are summarised in Figs. 8, 9 and 10. The rotation of the punch causes noticeable changes in the stress-strain state of the workpiece plate, see Fig. 8. Of particular interest is the emergence of a non-zero tangential velocity component orthogonal to ND. The punch rotation has relatively minor effect on hydrostatic pressure in the deformation zone, while significantly increases the amount and distribution of effective strain in the surrounding plate areas. Under the punch, hydrostatic pressure reaches $(2 \div 3)\sigma_s$, and in the annular zone around it $(1.5 \div 3)\sigma_s$. Effective strain has significant monotonic gradients in distribution from nil in the areas beyond approximately punch tip radius away from the punch to elevated in the immediate vicinity of the punch. The maximum level of strain can be found at the peripheral edge of a punch tip.

The level of accumulated strain as well as the other characteristics and their distribution strongly depend on contact friction, cf. Figure 9. As explained in the subsection (Method of finite-element (FE) simulations), the use of plastic friction coefficient $m=1$ in the FE simulations does not provide the condition of ultimate friction at the contact interface and therefore does not exclude the possibility of material sliding on the tool surface. To check this assumption, Fig. 9 reveals the results of FE simulations similar to those in Fig. 8 while calculated with $m=1.5$. It is striking to see an order of magnitude higher values of tangential velocity of the material flow at $m=1.5$ compared to that at $m=1.0$. With the punch rotation velocity of $0.5\ rad/s$, the material in its immediate vicinity flows with a maximum velocity of $v = 5\ mm \cdot\ 0.5s^{-1} = 2.5\ mm/s$ in the corner of tip stair – base transition, and gradually decaying in all directions away from it, Fig. 9. This estimate reveals that at m=1.5, the plate material virtually sticks to the punch surface at the tip stair – base transition, while slips at all the other surface areas, but much less intensively than at $m=1.0$. This has relatively minor effect on hydrostatic pressure in the deformation zone, while leads to an order of magnitude increase in the level of accumulated effective strain, see Fig. 9, albeit its distribution qualitatively similar to $m=1.0$ case.

These result are consistent with ref [28]. showing that in the FE simulations of HPT, an increase in the friction factor to $m=1.5$ eliminates saturation in the dependence of effective strain on the angle of dies rotation. In other words, workpiece is gripped by the die surfaces under such friction conditions [29].

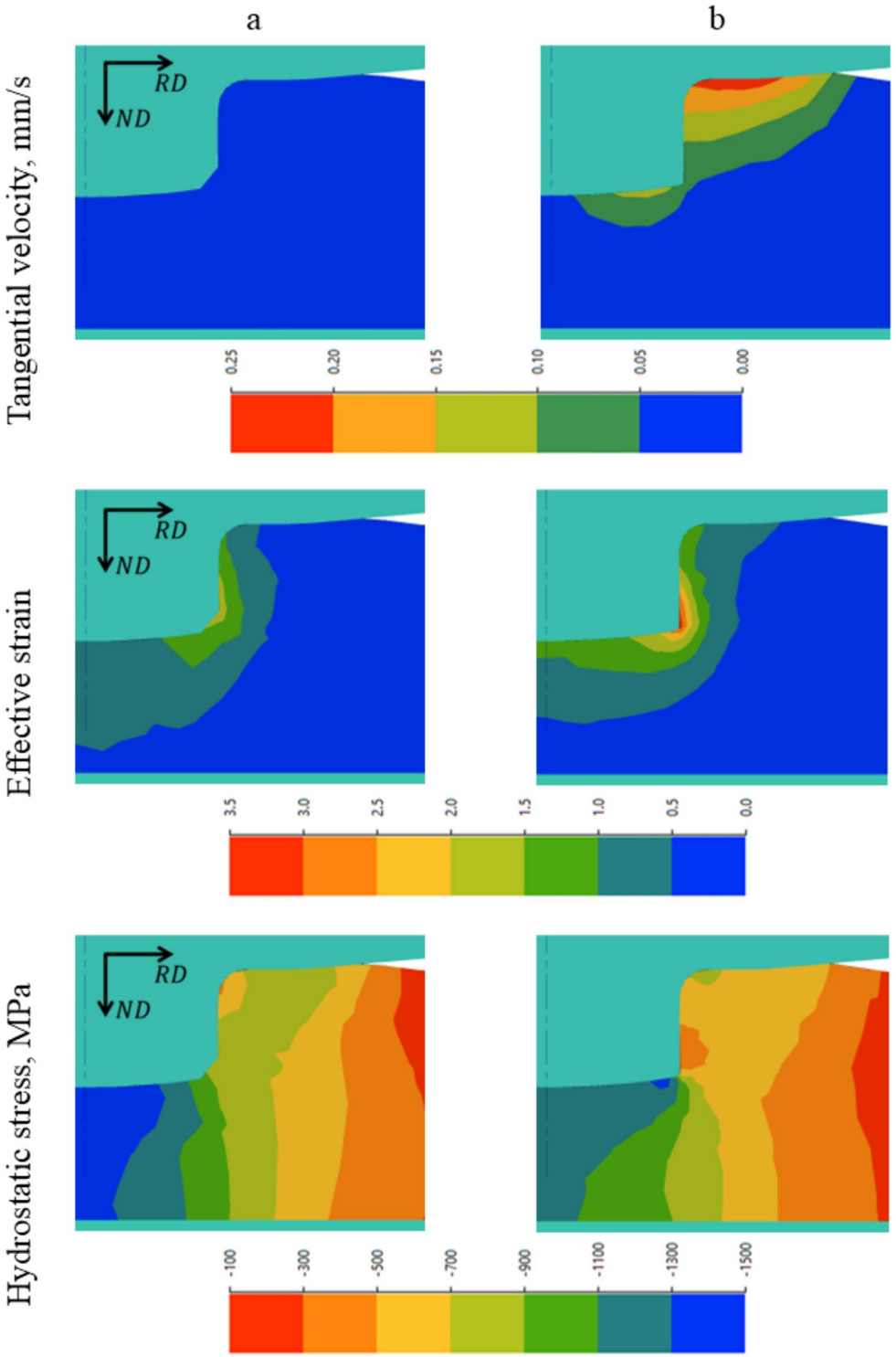

Fig. 8 FE simulation results showing the distributions of tangential velocity, effective strain and hydrostatic stress fields in the plate around the impingement area of non-rotating (**a**) and rotating for 3.3 revolutions (**b**) punches at $m=1$, translational and angular velocities of the punch 0.1 mm/s and 0.5 rad/s, respectively

Figure 10 shows the distribution of flow stress in AA5083 plate for a non-rotating Fig. 10a and a rotating Fig. 10b, c punches. It confirms that with a good grip, a rotating punch strain-harden the material in a much larger volume than a non-rotating counterpart. The increase of friction leads to a higher strain hardening.

Discussion

As has been shown in subsection (Numerical simulations), the rotation of the punch in L-HPT leads to an increase in the accumulation of effective strain, especially in the vicinity of punch tip at its peripheral edge and lateral surface,

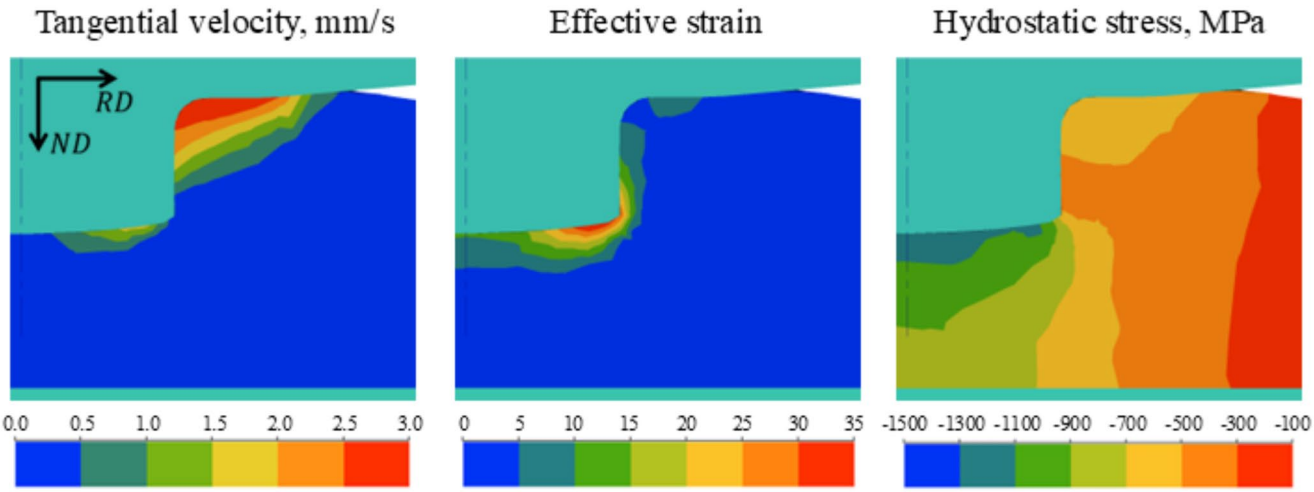

Fig. 9 FE simulation results showing the distributions of tangential velocity, effective strain and hydrostatic stress fields in the plate around the impingement area of rotating for 3.3 revolutions punch at $m = 1.5$, translational and angular velocities of the punch 0.1 mm/s and 0.5 rad/s, respectively

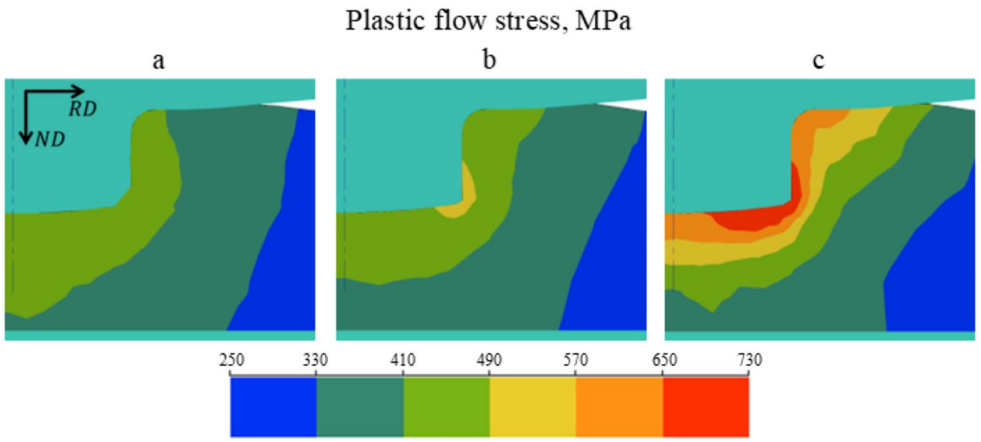

Fig. 10 Distribution of plastic flow stress [MPa] in the alloy AA5083 for non-rotating (**a**) and rotating for 3.3 revolutions punch (**b**, **c**) at translational and angular velocities of the punch 0.1 mm/s and 0.5 rad/s, respectively, and $f = 1.0$ (**a**, **b**) and $f = 1.5$ (**c**)

Fig. 8. With good adhesion at the punch-workpiece interface, i.e. high friction factor, this effect becomes more pronounced, Fig. 9, which leads to significant strain hardening, Fig. 10. These are very consistent with the experimental results presented in Sect. (Characterisation of microstructure) and (Microhardness mapping), and the distribution of microhardness in Fig. 7 in particular.

It is known that the gripping of a workpiece in HPT is possible only at a sufficiently high pressure, which should be several times higher than the flow stress of a workpiece material [20]. As we show above, the pressure at L-HPT is lower than that, but material gripping still takes place. We believe this is due to intense material flow in axial and radial directions. According to [29], such 'non-shear flows' significantly simplify the gripping of a workpiece material with a rotating punch.

The reported gradients in accumulated strain and flow stress distributions can be correlated with the velocity components of plastic flow field and should be discussed further. The tangential velocity component is equal to zero at the punch axis due to the process symmetry, linearly increases when moving away in radial direction, and then rapidly decreases to zero again beyond the punch periphery at the border of the deformation zone. The radial and axial components show a sharp turn from predominantly radial to axial flow at the punch lateral surface and is directed opposite to the punch motion. Such a material flow in L-HPT can be likened to that in twist extrusion (TE) [32] in terms of tangential motion with coinciding punch and extrusion axes, respectively. In terms of radial-axial flow, the thin radial layers of the deformation zone in L-HPT can be likened to the material flow in equal channel angular pressing (ECAP) [33] with the shear zone aligned parallel to the lateral punch surface. With such an orientation of deformation zones in respective techniques, both TE and ECAP create maximum strain in the areas of side surface of punch tip.

The dependence of effective strain under L-HPT on the process variables can be determined using dimensional

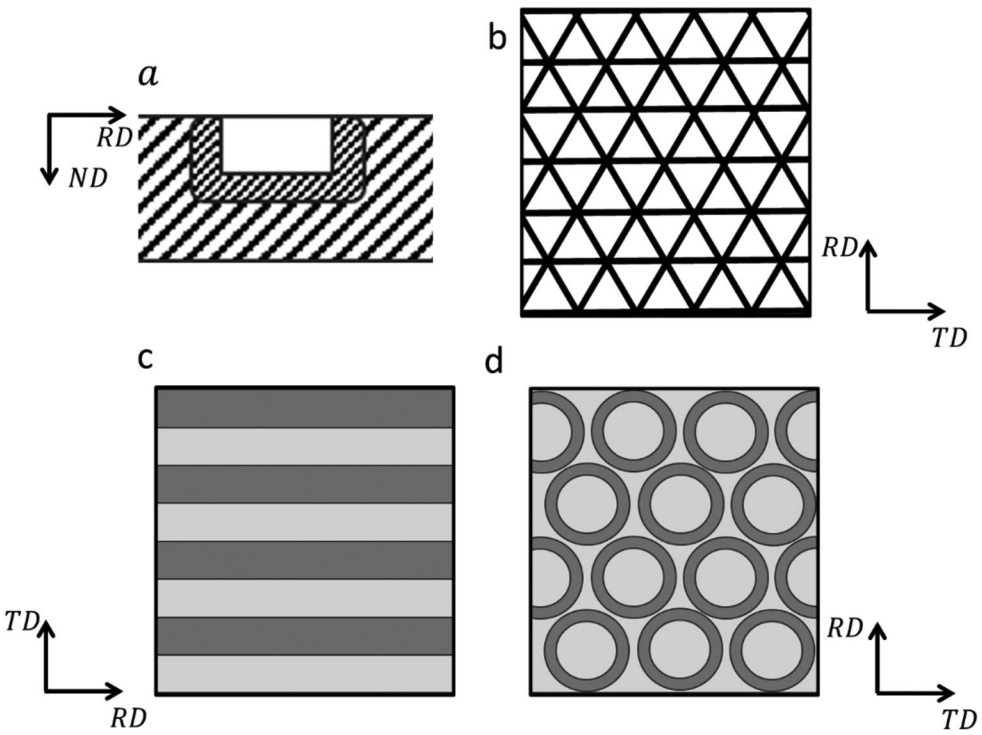

Fig. 11 Examples of heterostructure patterns that can be formed by L-HPT with darker areas indicating hardened material: (**a**) holes with hardened surfaces; (**b**) triangular mesh and (**c**) layered structure strengthening the plates and inhibiting the propagation of cracks; and (**d**) two-dimensional analogue of a harmonic structure (annular hardened zones created by a tubular punch)

theory [34]. Let us assume the deformation zone is localised around the area of punch impingement into the plate and is sufficiently far from the other surfaces. In this case, the size of the plate should not affect the amount of accumulated effective strain. Furthermore, let us consider the shape of the punch, the characteristics of a material and the contact friction conditions as given. In such a case, the variables defining the effective strain e_p are the punch velocities of axial translation V and angular rotation as well as the depth of its impingement into the plate L. According to the dimensional theory, we then obtain the following equation for the effective strain field.

$$e_p = (L/V)^a F\left(x/L, y/L, z/L\right) \tag{4}$$

,

where F is dimensionless function of dimensionless (normalised) spatial coordinates $x/L, y/L, z/L$, of the punch upon its impingement for a depth L, with a velocity V, which can be determined in an experiment. Assuming that e_p is directly proportional to a punch rotation angle, we obtain $a = 1$ and thus

$$e_p = LF/V \tag{5}$$

This relationship proves that the effective strain in the L-HPT process can be controlled by the variation of parameters V, , L.

The function $F\left(x/L, y/L, z/L\right)$ characterising the spatial distribution of effective strain in Eq. (4) is defined by the shape of the punch. For instance, the use of a hollow tube-shaped punch in L-HPT will allow creating ring-shaped areas of strain-hardened material. Of particular interest can also be punches allowing movements along the plate surface in the impinged state to form various patterns heterostructure (HS) zones in the plate. These can vary from isolated HS spots to architectures composed of HS lines to even more complex HS materials with 3D-architected structures assembled from patterned flat layers. Several examples of such materials are presented in Fig. 11 illustrating that L-HPT can be a very effective tool for creating architected heterostructures. Let us discuss here several possible applications further.

First, possible applications of L-HPT include plates with blind holes and locally hardened surfaces [35–37], Fig. 11a. Second, L-HPT created patterns can be 'reinforcement elements' like e.g. stiffeners in loaded plates, Fig. 11b, c. Finally, L-HPT can be used to create HS architectures in various metals alloys, e.g., planar analogues of harmonic-structure materials [5, 38], Fig. 11d.

Compared to composites, the main advantage of materials with architected HS is the homogeneity of chemical composition. Since elastic moduli are weakly dependant on grain structure, architected materials do not develop internal residual stresses under mechanical loading within elastic strain region, while the development of such reduces the strength of typical composites having chemically

heterogeneous components. For instance, HS architecture in the form of a triangular network (Fig. 11b) should increase the static strength of plates, while the layered architecture (Fig. 11c) should increase fracture toughness due to the suppression of crack propagation in soft plastic zones. Yet one more very important advantage of architected materials that are homogeneous in chemical composition is their recyclability, which eliminates the complex problem of separating components chemically.

Conclusions

A novel process 'Local High Pressure Torsion' (L-HPT) has been introduced in this work for imparting localised strain within workpiece surfaces. The process is based on impinging and driving a rotating punch in the workpiece surface.

On the example of one of the most common wrought aluminium alloys AA5083, the process has been proven experimentally to be very efficient in gripping and deforming peripheral layers of the workpiece material. This leads to the localised more than two-fold increase in material hardness compared to the base level in the workpiece bulk with rather sharp gradients. Maximal material hardness is found in the vicinity of peripheral edge and lateral surface junction of the punch tip.

Finite-element simulations of L-HPT process in QForm revealed that rotational flow of the workpiece material leads to the accumulation of shear strain. The latter increases with the increase of friction stress on the punch – workpiece contact. Further analysis based on dimensionality method shows that the level of effective strain for a given L-HPT tool geometry grows linearly with the increase of impingement depth, and is directly proportional to the ratio of rotation to impingement velocities.

L-HPT process allows creating on the workpiece surface severely deformed areas that can be locally isolated as well as continuously connected into desired patterns. Considering well-known advantages of architected heterostructures, L-HPT process opens new possibilities for creating materials with enhanced performance. The important peculiarity of such performance enhancement in various materials is the preservation of original chemical composition, which also improves possibilities for material recyclability and sustainability of our industrial technologies.

Acknowledgements The authors deeply appreciate the support of MICAS Simulations Ltd., Oxford, UK, for generously providing the QForm-3D software suite (version QForm UK 10.3.1) for finite-element analysis. YB thanks the Polish National Agency for Academic Exchanges (NAWA) for the financial support of this work within the Ulam NAWA program (Agreement BNI/ULM/2024/1/00008/U/DRAFT/00001), project "Heterostructure formation in metals by Rotating Indenter Technique".

Funding Open access funding provided by Lund University.

Data availability The authors declare that the data supporting the findings of this study are available within the paper. Raw data from the experiments presented in this work can be made available upon request.

Declarations

Conflict of interest The authors declare that they have no conflict of interest. The authors working for industrial companies (EB, YT, RF, IS, and NB) declare that respective companies also have no conflicts of interest associated with IP rights.

References

1. Ashby MF (2024) Materials selection in mechanical design, 6 ed., Butterworth-Heinemann
2. Sun Z, Zhou J, Retraint D (2023) Mechanical properties of metallic materials processed by surface severe plastic deformation. Mater Trans 64(8):1739–1753
3. Romero-Resendiz L, Naeem M, Zhu YT (2023) Heterostructured materials by severe plastic deformation: overview and perspectives. Mater Trans 64(10):2346–2360
4. Ameyama K, Cazes F, Couque H, Dirras G, Kikuchi S, Li J, Mompiou F, Mondal K, Orlov D, Sharma B, Tingaud D, Vajpai SK (2022) Harmonic structure, a promising microstructure design. Mater Res Lett 10(7):440–471
5. Orlov D, Ameyama K (2020) Critical assesment 37: harmonic-structure materials - idea, status and perspectives. Mater Sci Technol 36(5):517–526
6. Noronha DJ, Sharma S, Prabhu Parkala R, Shankar G, Kumar N, Doddapaneni S (2024) Deep rolling techniques: a comprehensive review of process parameters and impacts on the Material properties of Commercial Steels. Metals 14(6):667
7. Schulze V (2005) Modern mechanical surface treatment: States, Stability, effects. Wiley-VCH Verlag GmbH & Co. KGaA, Weinheim
8. Bajakke PA, Jambagi SC, Malik VR, Deshpande AS (2020) Friction stir Processing: an emerging Surface Engineering technique. In: Gupta K (ed) Surface Engineering of Modern materials. Springer International Publishing, Cham, pp 1–31
9. Mishra RS, Ma ZY (2005) Friction stir welding and processing. Mater Sci Engineering: R: Rep 50(1):1–78
10. Huang H, Niu J, Xing X, Lin Q, Chen H, Qiao Y (2022) Effects of the shot peening process on Corrosion Resistance of Aluminum Alloy: a review. Coatings 12(5):629

11. Zykova AP, Tarasov SY, Chumaevskiy AV, Kolubaev EA (2020) A review of Friction stir Processing of Structural Metallic materials: process, Properties, and methods. Metals 10(6):772
12. Wu X, Zhu Y, Lu K (2020) Ductility and strain hardening in gradient and lamellar structured materials. Scripta Mater 186:321–325
13. Butz GA, Lyst JO (1961) Improvement In Fatigue resistance of Aluminum Alloys by Surface Cold Working. Mater Res Stand 1961002
14. Zhu Y, Ameyama K, Anderson PM, Beyerlein IJ, Gao H, Kim HS, Lavernia E, Mathaudhu S, Mughrabi H, Ritchie RO, Tsuji N, Zhang X, Wu X (2021) Heterostructured materials: superior properties from hetero-zone interaction. Mater Res Lett 9(1):1–31
15. Edalati K, Ahmed AQ, Akrami S, Ameyama K, Aptukov V, Asfandiyarov RN, Ashida M, Astanin V, Bachmaier A, Beloshenko V, Bobruk EV, Bryła K, Cabrera JM, Carvalho AP, Chinh NQ, Choi I-C, Chulist R, Cubero-Sesin JM, Davdian G, Demirtas M, Divinski S, Durst K, Dvorak J, Edalati P, Emura S, Enikeev NA, Faraji G, Figueiredo RB, Floriano R, Fouladvind M, Fruchart D, Fuji M, Fujiwara H, Gajdics M, Gheorghe D, Gondek Ł, González-Hernández JE, Gornakova A, Grosdidier T, Gubicza J, Gunderov D, He L, Higuera OF, Hirosawa S, Hohenwarter A, Horita Z, Horky J, Huang Y, Huot J, Ikoma Y, Ishihara T, Ivanisenko Y, Jang J-i, Jorge AM, Kawabata-Ota M, Kawasaki M, Khelfa T, Kobayashi J, Kommel L, Korneva A, Kral P, Kudriashova N, Kuramoto S, Langdon TG, Lee D-H, Levitas VI, Li C, Li H-W, Li Y, Li Z, Lin H-J, Liss K-D, Liu Y, Cardona DMM, Matsuda K, Mazilkin A, Mine Y, Miyamoto H, Moon S-C, Müller T, Muñoz JA, Murashkin MY, Naeem M, Novelli M, Olasz D, Pippan R, Popov VV, Popova EN, Purcek G, de Rango P, Renk O, Retraint D, Révész Á, Roche V, Rodriguez-Calvillo P, Romero-Resendiz L, Sauvage X, Sawaguchi T, Sena H, Shahmir H, Shi X, Sklenicka V, Skrotzki W, Skryabina N, Staab F, Straumal B, Sun Z, Szczerba M, Takizawa Y, Tang Y, Valiev RZ, Vozniak A, Voznyak A, Wang B, Wang JT, Wilde G, Zhang F, Zhang M, Zhang P (2024) J Alloys Compd 1002:174667 J. Zhou, X. Zhu, Y.T. Zhu, Severe plastic deformation for producing superfunctional ultrafine-grained and heterostructured materials: An interdisciplinary review
16. Matsutani R, Sakuragi T, Yamagishi N, Miyazawa N, Nakada N, Onaka S (2021) SEM/EBSD Analysis of Grain Refinement and Coarsening of Ultra-fine-grained Al during simple Shear deformation. Mater Trans 62(7):921–928
17. Estrin Y, Vinogradov A (2013) Extreme grain refinement by severe plastic deformation: a wealth of challenging science. Acta Mater 61(3):782–817
18. Beygelzimer Y, Filippov A, Estrin Y (2023) Turbulent' shear flow of solids under high-pressure torsion. Phil Mag 103(11):1017–1028
19. Edalati K, Bachmaier A, Beloshenko VA, Beygelzimer Y, Blank VD, Botta WJ, Bryła K, Čížek J, Divinski S, Enikeev NA, Estrin Y, Faraji G, Figueiredo RB, Fuji M, Furuta T, Grosdidier T, Gubicza J, Hohenwarter A, Horita Z, Huot J, Ikoma Y, Janeček M, Kawasaki M, Král P, Kuramoto S, Langdon TG, Leiva DR, Levitas VI, Mazilkin A, Mito M, Miyamoto H, Nishizaki T, Pippan R, Popov VV, Popova EN, Purcek G, Renk O, Révész Á, Sauvage X, Sklenicka V, Skrotzki W, Straumal BB, Suwas S, Toth LS, Tsuji N, Valiev RZ, Wilde G, Zehetbauer MJ, Zhu X (2022) Nanomaterials by severe plastic deformation: review of historical developments and recent advances. Mater Res Lett 10(4):163–256
20. Zhilyaev AP, Langdon TG (2008) Using high-pressure torsion for metal processing: fundamentals and applications. Prog Mater Sci 53(6):893–979
21. Bridgman PW (1935) Effects of high shearing stress combined with high hydrostatic pressure. Phys Rev 48(10):825–847
22. Beygelzimer Y, Orlov D, Baretzky B, Estrin Y, Vinogradov A, Kulagin R (2024) Surface sliding revealed by operando monitoring of high-pressure torsion by acoustic emission. Mater Lett 363:136303
23. Edalati K, Horita Z, Langdon TG (2009) The significance of slippage in processing by high-pressure torsion. Scripta Mater 60(1):9–12
24. Limited MS (2024) QForm 3D. https://www.qform3d.com/. 2024.08.31)
25. Bomarito GF, Warner DH (2015) Micromechanical investigation of ductile failure in Al 5083-H116 via 3D unit cell modeling. J Mech Phys Solids 74:97–110
26. Nielsen CV, Bay N (2018) Review of friction modeling in metal forming processes. J Mater Process Technol 255:234–241
27. Levanov AN (1997) Improvement of metal forming processes by means of useful effects of plastic friction. J Mater Process Technol 72(2):314–316
28. Song Y, Wang W, Gao D, Yoon EY, Lee DJ, Kim HS (2014) Finite element analysis of the effect of friction in high pressure torsion. Met Mater Int 20(3):445–450
29. Beygelzimer Y, Estrin Y, Davydenko O, Kulagin R (2023) Gripping prospective of Non-shear flows under high-pressure torsion. Materials 16(2):823
30. Kachanov LM (2004) Fundamentals of the theory of plasticity. Dover, Mineola, NY, USA
31. Oguocha INA, Adigun OJ, Yannacopoulos S (2008) Effect of sensitization heat treatment on properties of Al–Mg alloy AA5083-H116. J Mater Sci 43(12):4208–4214
32. Beygelzimer Y, Varyukhin V, Kulagin R, Orlov D (2017) Twist extrusion. In: Rosochowski A (ed) Severe Plastic Deformation Technology. Whittles Publishing, Dunbeath, Scotland, pp 202–234
33. Valiev RZ, Langdon TG (2006) Principles of equal-channel angular pressing as a processing tool for grain refinement. Prog Mater Sci 51(7):881–981
34. Sedov LI (1993) Similarity and dimensional methods in mechanics, 10th edn. CRC
35. Hu B, Yoshida S, Gaffney J (2011) Stress and strain analysis of metal plates with holes, Springer New York, New York, NY, pp. 187–193
36. Almeida JHS, Bittrich L, Spickenheuer A (2020) Improving the open-hole tension characteristics with variable-axial composite laminates: optimization, progressive damage modeling and experimental observations. Compos Sci Technol 185:107889
37. Wang Z-Y, Wang Q-Y, Cao M (2017) Experimental study on fatigue Behaviour of Shot-Peened Open-Hole Steel plates. Materials 10(9):996
38. Sjögren-Levin E, Pantleon W, Ahadi A, Hegedüs Z, Lienert U, Tsuji N, Ameyama K, Orlov D (2024) Grain-level mechanism of plastic deformation in harmonic structure materials revealed by high-resolution X-ray diffraction. Acta Mater 265:119623

Terms and Conditions

Springer Nature journal content, brought to you courtesy of Springer Nature Customer Service Center GmbH (“Springer Nature”).
Springer Nature supports a reasonable amount of sharing of research papers by authors, subscribers and authorised users (“Users”), for small-scale personal, non-commercial use provided that all copyright, trade and service marks and other proprietary notices are maintained. By accessing, sharing, receiving or otherwise using the Springer Nature journal content you agree to these terms of use (“Terms”). For these purposes, Springer Nature considers academic use (by researchers and students) to be non-commercial.
These Terms are supplementary and will apply in addition to any applicable website terms and conditions, a relevant site licence or a personal subscription. These Terms will prevail over any conflict or ambiguity with regards to the relevant terms, a site licence or a personal subscription (to the extent of the conflict or ambiguity only). For Creative Commons-licensed articles, the terms of the Creative Commons license used will apply.
We collect and use personal data to provide access to the Springer Nature journal content. We may also use these personal data internally within ResearchGate and Springer Nature and as agreed share it, in an anonymised way, for purposes of tracking, analysis and reporting. We will not otherwise disclose your personal data outside the ResearchGate or the Springer Nature group of companies unless we have your permission as detailed in the Privacy Policy.
While Users may use the Springer Nature journal content for small scale, personal non-commercial use, it is important to note that Users may not:

1. use such content for the purpose of providing other users with access on a regular or large scale basis or as a means to circumvent access control;
2. use such content where to do so would be considered a criminal or statutory offence in any jurisdiction, or gives rise to civil liability, or is otherwise unlawful;
3. falsely or misleadingly imply or suggest endorsement, approval , sponsorship, or association unless explicitly agreed to by Springer Nature in writing;
4. use bots or other automated methods to access the content or redirect messages
5. override any security feature or exclusionary protocol; or
6. share the content in order to create substitute for Springer Nature products or services or a systematic database of Springer Nature journal content.

In line with the restriction against commercial use, Springer Nature does not permit the creation of a product or service that creates revenue, royalties, rent or income from our content or its inclusion as part of a paid for service or for other commercial gain. Springer Nature journal content cannot be used for inter-library loans and librarians may not upload Springer Nature journal content on a large scale into their, or any other, institutional repository.
These terms of use are reviewed regularly and may be amended at any time. Springer Nature is not obligated to publish any information or content on this website and may remove it or features or functionality at our sole discretion, at any time with or without notice. Springer Nature may revoke this licence to you at any time and remove access to any copies of the Springer Nature journal content which have been saved.
To the fullest extent permitted by law, Springer Nature makes no warranties, representations or guarantees to Users, either express or implied with respect to the Springer nature journal content and all parties disclaim and waive any implied warranties or warranties imposed by law, including merchantability or fitness for any particular purpose.
Please note that these rights do not automatically extend to content, data or other material published by Springer Nature that may be licensed from third parties.
If you would like to use or distribute our Springer Nature journal content to a wider audience or on a regular basis or in any other manner not expressly permitted by these Terms, please contact Springer Nature at

onlineservice@springernature.com